

# Formation of Platinum (Pt) Nanocluster Coatings on K-OMS-2 Manganese Oxide Membranes by Reactive Spray Deposition Technique (RSDT) for Extended Stability during CO Oxidation

Hector F. Garces<sup>1</sup>, Justin Roller<sup>2,3</sup>, Cecil K. King'ondou<sup>4</sup>, Saminda Dharmarathna<sup>5</sup>,  
Roger A. Ristau<sup>6</sup>, Rishabh Jain<sup>2,3</sup>, Radenka Maric<sup>2,3,7</sup>, Steven L. Suib<sup>5,6</sup>

<sup>1</sup>School of Engineering, Brown University, Providence, USA

<sup>2</sup>Department of Materials Science & Engineering, University of Connecticut, Storrs, USA

<sup>3</sup>Center for Clean Energy Engineering, University of Connecticut, Storrs, USA

<sup>4</sup>Department of Sustainable Energy Science and Engineering, Nelson Mandela African Institution of Science and Technology, Arusha, Tanzania

<sup>5</sup>Department of Chemistry, University of Connecticut, Storrs, USA

<sup>6</sup>Institute of Materials Science, University of Connecticut, Storrs, USA

<sup>7</sup>Chemical and Biomolecular Engineering Department, University of Connecticut, Storrs, US

Email: [Hector\\_Garces@brown.edu](mailto:Hector_Garces@brown.edu), [Justin.roller@engr.uconn.edu](mailto:Justin.roller@engr.uconn.edu), [rij11002@engr.uconn.edu](mailto:rij11002@engr.uconn.edu), [kithongo@gmail.com](mailto:kithongo@gmail.com),  
[dasaminda@gmail.com](mailto:dasaminda@gmail.com), [steven.suib@uconn.edu](mailto:steven.suib@uconn.edu), [ristau@ims.uconn.edu](mailto:ristau@ims.uconn.edu), [maric@engr.uconn.edu](mailto:maric@engr.uconn.edu)

Received October 23, 2013; revised November 23, 2013; accepted November 30, 2013

Copyright © 2014 Hector F. Garces *et al.* This is an open access article distributed under the Creative Commons Attribution License, which permits unrestricted use, distribution, and reproduction in any medium, provided the original work is properly cited. In accordance of the Creative Commons Attribution License all Copyrights © 2014 are reserved for SCIRP and the owner of the intellectual property Hector F. Garces *et al.* All Copyright © 2014 are guarded by law and by SCIRP as a guardian.

## ABSTRACT

Nanocluster formation of a metallic platinum (Pt) coating, on manganese oxide inorganic membranes impregnated with multiwall carbon nanotubes (K-OMS-2/MWCNTs), applied by reactive spray deposition technology (RSDT) is discussed. RSDT applies thin films of Pt nanoclusters on the substrate; the thickness of the film can be easily controlled. The K-OMS-2/MWCNTs fibers were enclosed by the thin film of Pt. X-ray diffraction (XRD), scanning electron microscopy/X-ray energy dispersive spectroscopy (SEM/XEDS), focus ion beam/scanning electron microscopy (FIB/SEM), transmission electron microscopy (TEM), and X-ray 3D micro-tomography (MicroXCT) which have been used to characterize the resultant Pt/K-OMS-2/MWCNTs membrane. The non-destructive characterization technique (MicroXCT) resolves the Pt layer on the upper layer of the composite membrane and also shows that the membrane is composed of sheets superimposed into stacks. The nanostructured coating on the composite membrane material has been evaluated for carbon monoxide (CO) oxidation. The functionalized Pt/K-OMS-2/MWCNTs membranes show excellent conversion (100%) of CO to CO<sub>2</sub> at a lower temperature 200°C compared to the uncoated K-OMS-2/MWCNTs. Moreover, the Pt/K-OMS-2/MWCNTs membranes show outstanding stability, of more than 4 days, for CO oxidation at 200°C.

## KEYWORDS

Manganese Oxide Membrane; Pt Nanostructures; Reactive Spray Deposition Technology (RSDT); Film Deposition; X-Ray Tomography

## 1. Introduction

Manganese oxide K-OMS-2 is a porous mixed-valent metal oxide with applications in catalysis [1-3], environmental remediation [4], sorption processes [5], and

microbial fuel cells [6]. The rationale for the synthesis of this octahedral molecular sieve (OMS) is based on its low cost, processability, stability, and excellent catalytic activity in different redox reactions [7]. Its processability permits the preparation of K-OMS-2 manganese oxide

materials composed of endless-type nanofibers that can readily be assembled into a paper or membrane [8]. This versatile free-standing structure in the form of a membrane is flexible, re-dispersible, foldable, moldable, and can be modified by ion-exchange, doping, distributed over large areas for clean-up as well as being used as a supporting structure to produce composite materials. Membranes are of special interest due to their porosity, permeability, and conductivity and hence their potential uses as sensors, catalysts, and in separation processes that remove bacteria, microorganisms, particulates, and organic material. Membranes can be assembled in several geometries facilitating the integration into different devices offering operational features unavailable with bulk materials [9]. Nano-composites of MWCNTs filled with  $\text{MnO}_2$  have already been prepared and the results show improvements in both electrochemical and conduction properties [10]. The MWCNTs improve the connectivity between electrochemical isolated metallic centers and the manganese oxide nano-wires in the membrane, resulting in enhancement in the electron transport properties throughout the porous materials. Cryptomelane manganese oxide K-OMS-2 is a promising material to use in batteries and shows good capacity to store electrical charge while also being inexpensive and environmentally friendly. The addition of MWCNTs to K-OMS-2 membranes is expected to improve the electrical, mechanical, and chemical resistance performance of the composite as well as to facilitate charge transfer.

Deposition of metals on K-OMS-2 membranes, in the open atmosphere, using a flame synthesis process has not been explored. This process constitutes a new cost-effective route to functionalize the inexpensive inorganic membrane and thereby incorporate new functionalities leading to improved performance in: capacitance, adsorption, and control over conversion and selectivity in catalysis.

Preparation of novel inorganic-organic composite materials and non-destructive characterization (NDC) has become very important in the field of materials science. NDC techniques permit the visualization of the component in load and the interaction with the host structure potentially reveals features commonly accessed only by time-demanding sample preparation procedures (*i.e.*, isolation in epoxy followed by polishing). Additionally, lightweight materials with catalytic activity used as supports have attracted much attention due to their synergistic effects; they drive reactions towards higher yields and increase the interaction between the substrate and support.

In this work, a simple, fast, and new deposition technique has been employed for the formation of a conformal, homogeneous coating of Pt on inorganic K-OMS-2 impregnated with MWCNTs (*i.e.*, the membrane sub-

strate). The coated membrane (Pt/K-OMS-2/MWCNTs) showed excellent catalytic activity at a relatively low temperature ( $200^\circ\text{C}$ ). Thin conformal films of Pt were deposited using Reactive Spray Deposition Technology (RSDT). RSDT is a direct, dry flame based synthesis process and is configured to deposit directly onto a K-OMS-2/MWCNT composite membrane [11-16]. RSDT is a method of depositing films through combustion of metal-organic or metal-inorganic compounds dissolved in a solvent, and has emerged as an analogue to other deposition techniques such as atomic layer deposition (ALD), chemical vapor deposition (CVD), pulse laser deposition (PLD), and physical vapor deposition (PVD). Some key advantages of the RSDT process over traditional processing methods are 1) a reduction in the number of processing steps required for catalyst formation, 2) avoiding wet processing routes, 3) lack of requirement for vacuum, 4) power consumption  $< 2$  kW, 5) ease of stoichiometry control by mixing of precursors in the liquid phase, 6) no drying cycle, and 7) direct deposition. The process essentially combines the catalyst production and film formation steps into one, takes place in the open atmosphere and eliminates the need to dispose of solvent waste; the solvent is completely combusted to  $\text{CO}_2$  and  $\text{H}_2\text{O}$ . **Figure 1** (left) shows a schematic of the RSDT process. The figure on the right shows the deposition hardware set-up for thin film deposition.

Formation of nanocrystallites, via the RSDT technique, occurs through a sequential growth process that involves multiple intermediate steps. Nucleation occurs from the vapor phase whereby the metal or metal oxide grows into a primary particle during residence, along the length of the hot reactive zone [17]. There may be several pathways through which the vaporized metal reacts, nucleates, and grows either during time of flight or directly onto the substrate [18].

The precursor, once the droplet exits from the nozzle, proceeds through the following steps: heats up to the boiling point of the solvent; precipitates due to a rapid solvent shell volume decrease (*i.e.*, simultaneous evaporation and combustion); decomposes; phase changes from solid to vapor; and finally undergoes a series of redox reactions.  $\text{Pt}^{2+}$  is reduced to Pt metal. Formation of the

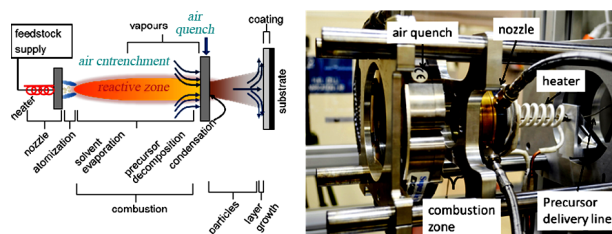


**Figure 1.** Schematic diagram of the RSDT process (left), and a mirror image of the process as set-up for deposition, substrate not shown (right).

nanocrystallite particles, during time-of-flight, occurs prior to film formation through a multi-step process on a time scale of milliseconds. The general mechanism of particle growth, once the precursor has vaporized, occurs by: homogeneous reactions, nucleation, surface growth, cluster dynamics (a transitory state between single atoms and solid material), coalescence, aggregation, and agglomeration [19]. The solid particle passes through the following size classifications during the growth process: monomer formation, cluster, primary particle, nanoparticle, and then agglomerate [19-21]. Depending on the processing conditions, a film can form from the vapor phase (*i.e.*, the product reaches the substrate at a stage somewhere between the monomer and nanoparticle pathway), either by a physical impingement of a fully formed nanoparticle (*i.e.*, a ballistic collision), or by a combination of both mechanisms.

The exact mechanism of growth is affected by the residence time in a given thermal profile, concentration of reactants, the precursor composition, oxidant/fuel flow rates, and the distance between the substrate and the nozzle. The thermal profile is controlled by the equivalence ratio, choice of fuel, quench distance, stand-off distance, flow rate, and nozzle design. Primary particle growth is arrested through rapid cooling using an air quench, to create a fast non-equilibrium phase change [22]. The time of flight, zone temperature profile, stand-off distance, and locations of the quench are critical to formation of the desired metal and morphology [19].

## 2. Experimental

### 2.1. Manganese Oxide Inorganic Membrane Synthesis

The inorganic K-OMS-2 membrane was prepared as previously reported [8]. Briefly, 11.37 g of potassium sulphate ( $K_2SO_4$ ), 17.64 g of potassium persulphate ( $K_2S_2O_8$ ), 7.35 g of manganese sulfate monohydrate ( $MnSO_4 \cdot H_2O$ ), and 70 mL of distilled deionized water (DDW) are mixed together in a Teflon liner and placed in an autoclave at 250°C for 4 days in a conventional oven. After the synthesis, the material was dispersed in DDW. The K-OMS-2/MWCNTs composite membrane was formed after purification of the MWCNTs using an acid method procedure [23]. Briefly, the MWCNTs were boiled in concentrated (68%)  $HNO_3$  at 120°C under reflux for about 48 h, washed with DDW,  $NH_4OH$ , DDW,  $HCl$ , DDW, filter, and finally dried. Finally, about 3.5 wt% of the purified MWCNTs was re-dispersed with the K-OMS-2 fibers to obtain the composite membrane.

### 2.2. Deposition of Pt on K-OMS-2 Membrane

Metallic platinum was deposited on modified K-OMS-2 membranes with MWCNTs by reactive spray deposition

technology (RSDT). Briefly, the method involved pumping platinum acetylacetonate (PtAcac) dissolved in a toluene/propane solvent (20 wt% propane) through an atomizing nozzle at a flow rate of 4 mL/min and combusting the atomized spray (Figure 1). The deposition zone was directed onto a 4 mm × 4 mm K-OMS-2/MWCNTs substrate occurred by impinging the flame on the substrate at a stand-off distance of 15 cm. The PtAcac was dissolved into toluene and further diluted with propane to a final metal concentration of 6.1 mm. The solution was heated in the atomizing nozzle via induction to a temperature of 170°C. The solvent was passed through the nozzle at an average pressure of 190 psi, producing a flame approximately 7.5 cm long. A sheath of oxygen surrounded the atomized spray at a flow rate of 12 slpm. The average substrate temperature was 100°C during the deposition.

### 2.3. K-OMS-2 Membrane Characterization

X-ray diffraction analysis was performed to evaluate the nature of the as prepared membrane, and after deposition of Pt on the modified membrane. The inorganic membranes were analyzed in an Ultima IV Rigaku X-ray diffractometer (Cu  $K\alpha$  radiation). Diffraction patterns were obtained in the range of 5 - 75  $2\theta$  degrees at a scan rate of 2°  $min^{-1}$ . Scanning electron microscopy (SEM) was performed in an FEI Quanta ESEM 250 scanning electron microscope. The sample was cut in a square of about 5 mm and placed in a carbon tape. A cross section of the Pt deposited on the substrate was made after immersing a piece Pt/K-OMS-2/MWCNTs in an epoxide, and polishing with 1200, 600, and 320 grit grinding paper, and polishing with 5  $\mu m$ , 3  $\mu m$ , 1  $\mu m$ , and 0.3  $\mu m$  alumina powders, and 0.1 silica dispersion in a cloth sheet. Mapping of the samples were obtained by energy dispersive X-ray analysis (EDAX) in an FEI Quanta ESEM 250 operated at 20.0 kV with X-ray spectra acquired and processed with an Ametek Genesis Apex 4. High temperature scanning electron microscopy (HTSEM) was performed in an FEI Quanta ESEM 250 scanning electron microscope. Membrane type Pt/K-OMS-2/MWCNTs were heated to the analysis temperature at 50°C  $min^{-1}$  and stabilized for 30 minutes before an SEM image was taken. FIB/SEM images were acquired using The Strata 400 STEM Dual-Beam system equipped with Focused Ion Beam (FIB) technology and a Flipstage/STEM assembly. This system permits complete in situ sample preparation and high-resolution analysis. Transmission electron microscopy (TEM) micrographs were obtained using a JEOL JEM 2010 FasTEM operating at 200 kV. The specimens were loaded onto a carbon-coated gold grid. High resolution X-ray 3D tomography was performed in a MicroXCT-400. The specifications for the tomography employed a 40 keV accelerating voltage and a beam current of 4 W.

Two thousand projections were collected from  $-90$  to  $90$  theta with an exposure time of 14 second per image. Reconstruction and visualization employed were performed afterwards.

## 2.4. CO Oxidation

The CO oxidation in a temperature range from  $50^{\circ}\text{C}$  to  $400^{\circ}\text{C}$  employed a vertical fixed-bed tubular reactor made of quartz with an internal diameter of 4 mm. In each experiment, the membrane was cut into square pieces of about 1 mm, packed in the quartz reactor, and held by quartz wool in both ends. The catalyst was heated to the analysis temperature with an Ar down flow of 40 CCM and held for 30 minutes before the beginning of the CO oxidation. Afterwards, three consecutive automatic injections were sampled at each evaluation temperature. The analytical system comprised an Agilent 3000 Micro GC equipped with two thermal conductivity detectors. A Molecular Sieve and a Plot Q capillary column were used for the separation. Tubing and fittings were stainless steel throughout. In each experiment, about 0.06 g of K-OMS-2/MWCNTs and Pt/K-OMS-2/MWCNTs catalyst was placed in the reactor supported by quartz wool. A furnace with PID control held the reactor temperature constant. The thermocouple was placed at the top of the catalyst bed. Mass flow controllers (MFC) were used to control flow rates, feed, and composition. A certified gas mixture (Airgas; 10% CO in  $\text{N}_2$ ), pure  $\text{O}_2$  and Ar as balance were used for the CO oxidation. Stability tests for CO oxidation were performed at  $200^{\circ}\text{C}$ . For the stability test, the reactor containing the catalyst (Pt/K-OMS-2/MWCNTs) was ramped to  $200^{\circ}\text{C}$ , purged for 30 minutes with Argon down flow, and kept for about 4 days for the analysis. After the purging, 3 simultaneous sampling injections at different time intervals were directed into the column and the outlet concentrations were averaged.

## 3. Results and Discussion

### 3.1. X-Ray Diffraction

The diffraction patterns for the K-OMS-2/MWCNTs, and the Pt deposited membrane (Pt/K-OMS-2/MWCNTs) are presented in **Figure 2**. Diffraction patterns (a) for the impregnated K-OMS-2 with MWCNTs correspond to the tetragonal manganese oxide K-OMS-2 cryptomelane phase (ICSD No. 01-070-8072). Peaks for face centered cubic metallic Pt can be observed after deposition by RSDT [**Figure 2(b)** Pt/K-OMS-2/MWCNTs]. 1.17 wt % of metallic platinum was loaded in the composite membrane. Diffraction peaks for the platinum phase deposited on a bare aluminum stub as a control during the deposition by RSDT and X-ray diffraction patterns of cryptomelane manganese oxide and metallic platinum with a

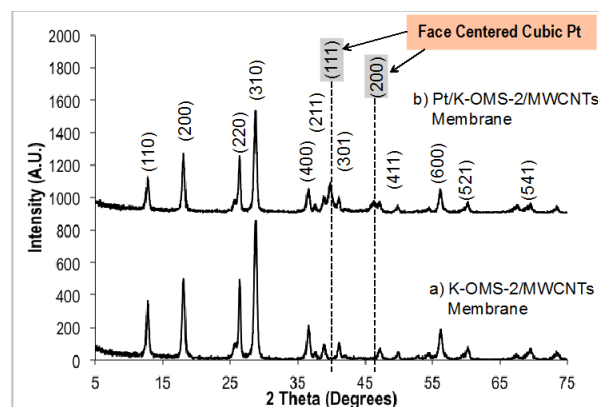


**Figure 2.** X-ray diffraction patterns of (a) fresh K-OMS-2/MWCNTs and (b) Pt/K-OMS-2/MWCNTs. Diffractions peaks correspond to cryptomelane type manganese oxide (ICSD No. 01-070-8072) and metallic platinum face centered cubic (ICDD No. 00-004-082).

face centered cubic structure (ICDD No. 00-004-082) plotted using crystal maker software [24] are in accordance with the results (Supporting Information, **Figures S1, S2**).

The Pt precursor deposited on the K-OMS-2/MWCNTs membrane material was completely and successfully transformed into crystalline metallic Pt coating as depicted by the X-ray diffraction pattern, **Figure 2**. The reflections that correspond to metallic platinum (111) and (200) are clearly observed at angles of about  $39.5$  and  $46.0$  degrees two-theta respectively, along with the manganese oxide K-OMS-2 cryptomelane type material XRD peaks, **Figure 2(b)**. The platinum acetylacetonate (PtAcac) precursor was not detected after the deposition; this indicates a complete decomposition during the deposition. Additionally, the substrate temperature, due to the exothermic combustion from the torch, did not destroy the K-OMS-2 support. The substrate temperature was held constant at  $100^{\circ}\text{C}$  and the stand-off distance between the nozzle and substrate was held at 15 cm. The stability of the support after exposure to the reactive zone is confirmed by the post-deposition XRD pattern, which shows the pristine tetragonal phase of the K-OMS-2, (ICSD No. 01-070-8072). The interaction of the heat, from the flame, with the substrate does not induce structural changes; the crystal structure of the manganese oxide was preserved. Cryptomelane-type manganese oxide (K-OMS-2) materials are stable up to  $800^{\circ}\text{C}$  depending on the synthetic conditions under which they are prepared [25]. Therefore, unlike using the RSDT technique reported herein, loading active components on K-OMS-2 materials using high temperature deposition methods would certainly transform the cryptomelane type structure to more stable phases such as  $\text{Mn}_2\text{O}_3$ . Consequently, several physical properties, including its mixed-valence nature, would be altered and adversely affect catalytic activity. The sub-

strate can be kept at relatively low temperatures (e.g.  $<150^{\circ}\text{C}$ ) by controlling the proximity of the torch to the substrate; this stand-off avoids unwanted phase transformations, or oxidation of components in the composite such as the carbon nanotubes. At the same time, the system is flexible allowing the possibility to deposit materials on a substrate maintained at high temperatures by an external heating device or nearing the torch during the deposition. At one extreme the luminous tip of the flame could be impinged directly onto the substrate creating temperatures around  $800^{\circ}\text{C}$ .

### 3.2. Scanning Electron Microscopy

Scanning electron microscopy (SEM) images are shown in **Figure 3**. Micrographs (a), (b) and (c), (d) are for the fresh K-OMS-2/MWCNTs membrane and Pt/K-OMS-2/MWCNTs after RSDT deposition of Pt, respectively. The membrane material is composed of individual fibers with different diameters, some of them as low as 20 nm and several microns in length that intertwined in different directions forming a porous blanket, **Figures 3(a), (b)**. Surface fibers are homogeneously coated in Pt, by RSDT, showing an island growth morphology around the former K-OMS-2/MWCNTs composite membrane. Empty sections on the surface of the blanket of fibers are absent, **Figures 3(c), (d)**. X-ray energy dispersive spectroscopy (XEDS) mapping of a cross section of the coated membrane and focus ion beam scanning electron microscopy (FIB/SEM) images are presented in **Figure 4**. Layers of superimposed K-OMS-2 that form a stack are evident in the cross sectional image, **Figure 4(a)**. EDS mapping of the cross section shows a thick layer of Pt in the upper section of the membrane along with elements that con-

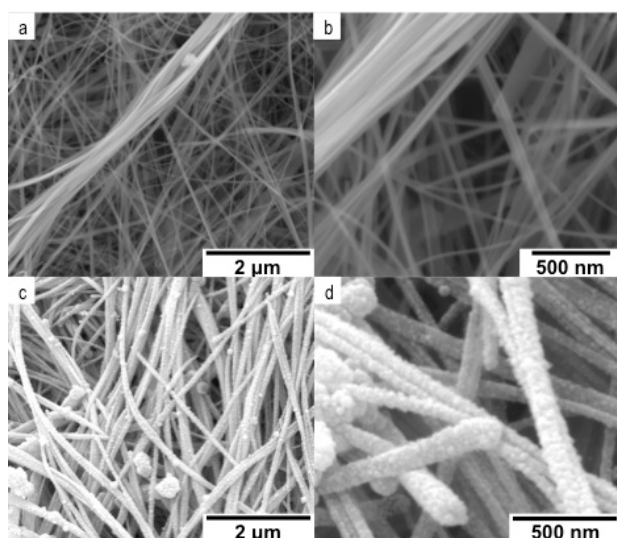


**Figure 3.** Scanning electron microscopy images of (a), (b) K-OMS-2/MWCNTs before coating, and (c), (d) Pt/K-OMS-2/MWCNTs after Pt deposition by RSDT.

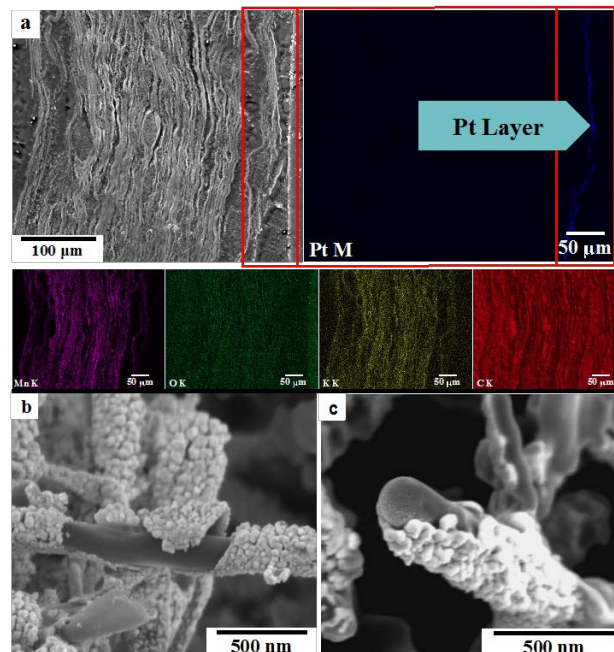


**Figure 4.** Scanning electron microscopy of (a) cross section of Pt/K-OMS-2/MWCNTs and EDX mapping, and (b), (c) focus ion beam scanning electron microscopy (FIB/SEM) of coated Pt/K-OMS-2/MWCNTs.

stitute K-OMS-2 in the inner layers. The coating of metallic Pt that wraps the composite K-OMS-2/MWCNTs fibers is up to 60 nm thick, **Figures 4(b), (c)**.

A uniform coating of Pt covered the upper fibers of K-OMS-2/MWCNTs membrane, **Figures 3(c), (d)**. The resultant conformal film of Pt nanoclusters covered the individual fibers on the upper-side of the membrane completely, without inducing any fiber aggregation. Moreover, the Pt coating did not cover the interstitial spaces between fibers substantially and this preserved the porous nature of the substrate (Supporting Information, **Figure S3**); this is a property critical to the catalytic performance. High temperature scanning electron microscopy (HTSEM) of a selected area also shows no change in morphology or sintering, agglomeration, and delamination of the coated Pt film with temperature. Possible decomposition of unreacted reagents after the deposition was also not observed (Supporting Information, **Figure S4**). This observation confirms that RSDT, which operates in the open atmosphere, can effectively be employed to functionally deposit controlled films on metal oxide inorganic membrane supports or composites without leaving undesirable by-products that might poison the functionalized oxide thereby decreasing their activity in their intended applications. Focused ion beam scanning electron microscopy (FIBSEM) revealed that the Pt film is constructed of small clusters of less than 50 nm in size that form a shell over the manganese oxide fibers and carbon nanotubes as shown by the FIBSEM micrographs

in **Figures 4(b), (c)**, that show a debonded Pt film after FIB sectioning. The Pt coat would, otherwise, not come apart after being deposited and would not leave the fibers exposed in the upper layer of the K-OMS-2/MWCNTs membrane. Additionally, deposition by RSDT produces a conformal film, which indicates the capability of the deposition method to permeate porous structures thereby facilitating the complete coverage of the substrate.

### 3.3. X-Ray 3D Tomography

X-ray 3D tomography resolved the layer of platinum deposited on the K-OMS-2/MWCNTs membrane, **Figure 5**. It is also observed, as by SEM imaging of a cross section, that the membrane is composed of superimposed layered sheets that form a stack. The X-ray absorption levels of the different components of the composite system define the structure. The contrast between the high (Pt) and the low absorption manganese material in the membrane are well resolved. There is no dispersion of Pt in the inorganic matrix, only the upper manganese oxide layer got covered by the nanostructured array of metallic Pt, **Figure 5(a)**. The orthogonal view of the 3D image also illustrates the layered structure of the inorganic matrix, **Figures 5(b)-(d)**.

Resolving the layered nature of the Pt/K-OMS-2/MWCNTs membrane involves destructive techniques with high energy Argon ions beam (FIB/SEM) and/or other time consuming procedures, that might involve embedding the material in epoxies that go through a time consuming polishing procedure to access the material in order to image it (**Figure 4(a)**). Unlike in the above-mentioned techniques, this work presents a non-destructive technique that not only resolves the upper layer of the coated material but also permit the visualization of the stacking layers of the inorganic constituent, K-OMS-2, that forms the composite membrane material. Considering the attenuation of X-rays by dense bodies, carbon (C,

$Z = 6$ ) cannot be accessed. However, the contrast between the high atomic number Pt material (Pt,  $Z = 78$ ) deposited, and the low atomic number elements that constitute the layered manganese oxide membrane (Mn,  $Z = 25$ ; K,  $Z = 19$ ; O,  $Z = 8$ ) are well resolved.

The use of X-ray tomography in materials science has been recently applied to study the 3D microstructural interactions in materials [26-31], and has become an important characterization technique with three-dimensional output information about the embedded phase, size, shape, and orientation.

**Figure 5(a)** presents the X-ray 3D tomography for the Pt/K-OMS-2/MWCNTs showing the layer of Pt deposited on the membrane material and the stacking of layers of sheets that make up the membrane. The 3D orthogonal view (**Figure 5(d)**) shows wavy lines along each orthogonal plane merging to form the stack of the layers. This can also be observed in **Figure 5(b)**. The resolution of the instrument used for the 3D tomography ( $\sim 0.5 \mu\text{m}$ ) does not resolve the nanometer size of the individual fibers that compose the composite membrane but presents a clear picture at the micron scale of the organization of the material inside the membrane. The X-ray absorption levels of the components attenuated on the composite define the structure. There is no dispersion of Pt in the inorganic K-OMS-2 matrix; only the upper layer was covered by the nanostructured array of metallic Pt, **Figure 5(a)**. Although the membrane is permeated by Pt to form the conformal structure, this permeation only penetrates into a few upper layers. Increases in the thickness of the coated material, in the upper layer, with deposition time eventually reduce the permeation to the lower layers. This closes paths for the platinum and restricts access to layers of K-OMS-2/MWCNTs underneath; the functionalized Pt material is therefore restricted to a few microns at the surface of the substrate. This technique is therefore self-limiting in terms of substrate penetration. The purpose of the tomographic analysis is to highlight the internal microstructure of the substrate; the coated layer; and to gain an understanding of the interaction between the support and the host structure. The deposition is homogeneous along the support structure.

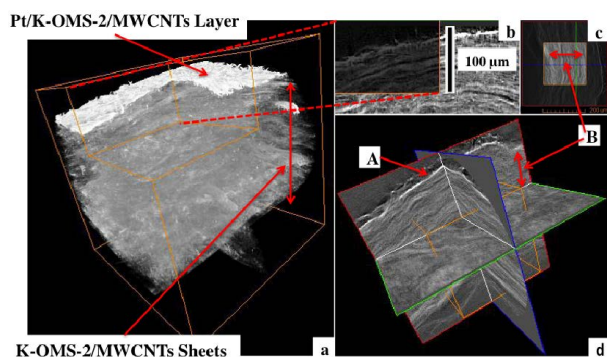


**Figure 5.** X-ray 3D micro tomography of (a) Pt/K-OMS-2/MWCNTs and layer of inorganic K-OMS-2 in the membrane and (b), (c) Pt/K-OMS-2/MWCNTs layers, (d) three orthogonal slices of Pt/K-OMS-2/MWCNTs showing Pt/K-OMS-2/MWCNTs (A), and K-OMS-2 layers (B).

### 3.4. Transmission Electron Microscopy

Further morphological and crystal structure studies by transmission electron microscopy (TEM) are presented in **Figure 6**. Low magnification TEM image show K-OMS-2 fibers and carbon nanotubes merged together and both hold platinum nanoparticles during the RSDT coating, **Figures 6(a), (b)**. Individual fibers of K-OMS-2 with diameters of about 20 nm and length extending to several microns with some of them sticking together forming a bundle were observed, **Figure 6(b)**. A high-resolution TEM (HRTEM) micrograph (**Figure 6(c)**) shows that the

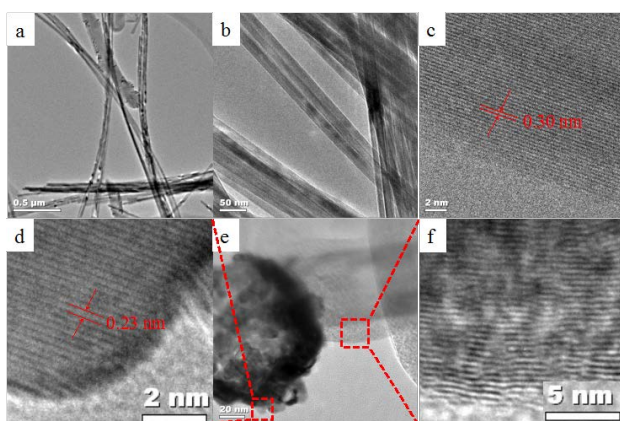


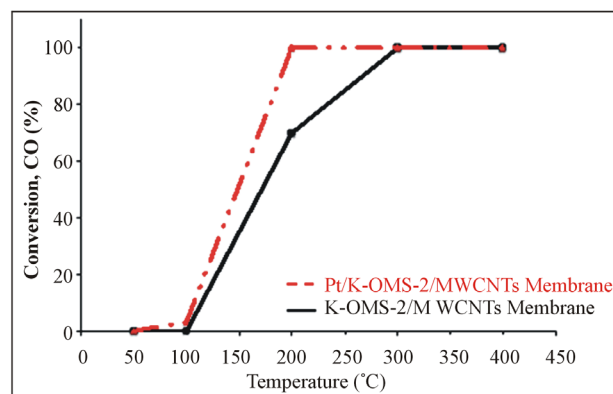
**Figure 6.** Transmission electron microscopy of (a) K-OMS-2 fibers and carbon nanotubes, (b) fibers of K-OMS-2, (c) K-OMS-2 with periodic lattice fringes of 3.0 Å corresponding to the inter-planar spacing of (310) planes, (d) Pt particle hosted by a MWCNTs with lattice fringes of 2.3 Å corresponding to the (111) planar spacing for metallic platinum, (e) MWCNTs hosting the Pt particles, and (f) lattice fringes of MWCNTs.

K-OMS-2 nanofibers are single crystalline with periodic lattice fringes of 3.0 Å corresponding to the inter-planar spacing of (310) planes. In **Figure 6(e)**, HRTEM image shows a MWCNT hosting a coated Pt particle. The coated Pt particle shows lattice fringes of 2.3 Å corresponding to the (111) planar spacing for metallic platinum. The inter-planar spacings observed are all in accordance with those measured with XRD for the bulk powdered sample for both the K-OMS-2 and metallic Pt materials.

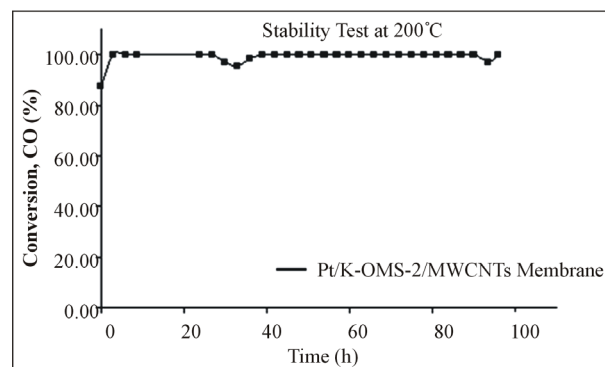
As shown by HRTEM, Pt nanoparticles are distributed on both the K-OMS-2 fibers and MWCNTs, **Figure 6(a)**. The coverage of the Pt film in the TEM micrographs is not homogeneous since the sample preparation procedure to obtain HRTEM images of the Pt/K-OMS-2/MWCNTs membrane involved cutting the sample with a diamond blade, sonication, and depositing the sample onto a copper grid. As a result, many of the Pt particles peeled off from the surface of the K-OMS-2/MWCNTs fibers during this procedure. However, some of the platinum particles that do remain exhibit a size of about 15 nm (**Figure 6(a)**; Supporting Information, **Figure S5**).

### 3.5. Carbon Monoxide (CO) Oxidation

Carbon monoxide (CO) oxidation is presented in **Figure 7** in the range 50°C - 400°C. Lower temperatures ( $\leq 200^\circ\text{C}$ ) were found to be optimal for high CO conversion with the coated Pt/K-OMS-2/MWCNTs material than the uncoated K-OMS-2/MWCNTs, reaching 100% conversion at 200°C. Higher temperatures ( $\geq 300^\circ\text{C}$ ) resulted in 100% conversion for both materials. A stability test at 200°C for CO oxidation shows that the coated Pt/K-OMS-2/MWCNTs remains active without apparent activity decrease



(a)



(b)

**Figure 7.** Carbon monoxide (CO) oxidation for (a) coated platinum Pt/K-OMS-2/MWCNTs and uncoated K-OMS-2/MWCNTs, (b) stability test at 200°C for Pt/K-OMS-2/MWCNTs during 96 h.

for more than 4 days (**Figure 7(b)**).

Carbon monoxide oxidation is catalyzed by a wide variety of materials [32-41]. Several of these materials are supported on high temperature ceramics to impart mechanical, thermal resistance, and to avoid depletion of the active metal. Platinum is one of the most commonly used metals for CO oxidation. Pt is stable, resistant to moisture, and highly active for the formation of CO<sub>2</sub> [32,33,35]. The use of membranes is limited for these purposes in part because they cannot withstand larger pressure levels, limiting operational flexibility, and the use of higher pressures and in some cases the upper temperature. However, low drop pressures, flexibility, and permeation are some of the advantages that these structures can offer. The loading of Pt on K-OMS-2/MWCNTs composite membranes reflects the versatility in using a composite structure; these options incorporate different materials that impart flexibility in the membrane design and enhance other properties such as conduction. Pt coated membrane, Pt/K-OMS-2/MWCNTs showed higher activity than the uncoated K-OMS-2/MWCNTs, reaching 100% conversion not only at low temperature (200°C) but also being highly stable over a long period of time at 200°C, with no

apparent degradation in catalytic conversion.

#### 4. Conclusion

A simple, fast, and new deposition technique has been employed for the formation of highly homogeneous conformal Pt coatings on an inorganic K-OMS-2/MWCNTs composite membrane. The deposition of Pt obtained by RSDT, reduces the number of processing steps required for catalyst formation into one step in the open atmosphere, and eliminates the solvent disposal problem. Additionally, RSDT is a controllable carrier concentration, where the thickness of the layer can be built up from the precursor solution. The resultant Pt/K-OMS-2/MWCNTs membrane has been used for the CO oxidation over a wide temperature range (RT-400°C) without degradation of the coating. The functionalized membrane showed great performance and stability (>4 days) at lower temperatures than the uncoated one. This work also presents an alternative use for K-OMS-2 in the form of membranes incorporating this composite in catalytic processes. The work also presented a non-destructive characterization technique for the visualization of the high X-ray absorbing metallic phase supported in the nanomaterial K-OMS-2 phase. The technique resolved the coating layer and the nature of the inorganic K-OMS-2 membrane with minimal time-consuming sample preparation procedures.

#### Acknowledgements

We thank the Chemical Sciences, Geosciences, and Biosciences Division, Office of Basic Energy Sciences, Office of Sciences of the US Department of Energy for support of this work.

#### REFERENCES

- [1] C. K. King'ondou, N. Opembe, C. Chen, K. Ngala, H. Huang, A. Iyer, H. F. Garces and S. L. Suib, "Manganese Oxide Octahedral Molecular Sieves (OMS-2) Multiple Framework Substitutions: A New Route to OMS-2 Particle Size and Morphology Control," *Advanced Functional Materials*, Vol. 21, No. 2, 2011, pp. 312-323. <http://dx.doi.org/10.1002/adfm.201001020>
- [2] A. Iyer, J. Del-Pilar, C. K. King'ondou, E. Kissel, H. F. Garces, H. Huang, A. M. El-Sawy, P. K. Dutta and S. L. Suib, "Water Oxidation Catalysis Using Amorphous Manganese Oxides, Octahedral Molecular Sieves (OMS-2), and Octahedral Layered (OL-1) Manganese Oxide Structures," *Journal of Physical Chemistry C*, Vol. 116, No. 10, 2012, pp. 6474-6483. <http://dx.doi.org/10.1021/jp2120737>
- [3] S. Dharmarathna, C. K. King'ondou, W. Pedrick, L. Pahalagedara and S. L. Suib, "Direct Sonochemical Synthesis of Manganese Octahedral Molecular Sieve (OMS-2) Nanomaterials Using Cosolvent Systems, Their Characterization, and Catalytic Applications," *Chemistry of Materials*, Vol. 24, No. 4, 2012, pp. 705-712. <http://dx.doi.org/10.1021/cm203366m>
- [4] M. Abecassis-Wolfovich, R. Jothiramalingam, M. V. Landau, M. Herskowitz, B. Viswanathan and T. K. Varadarajan, "Cerium Incorporated Ordered Manganese Oxide OMS-2 Materials: Improved Catalysts for Wet Oxidation of Phenol Compounds," *Applied Catalysis B: Environmental*, Vol. 59, 2005, pp. 91-98. <http://dx.doi.org/10.1016/j.apcatb.2005.01.001>
- [5] B. Hu, C. Chen, S. J. Frueh, L. Jin, R. Joesten and S. L. Suib, "Removal of Aqueous Phenol by Adsorption and Oxidation with Doped Hydrophobic Cryptomelane-Type Manganese Oxide (K-OMS-2) Nanofibers," *Journal of Physical Chemistry C*, Vol. 114, 2010, pp. 9835-9844. <http://dx.doi.org/10.1021/jp100819a>
- [6] X. Li, B. Hu, S. L. Suib, Y. Lei and B. Li, "Electricity Generation in Continuous Flow Microbial Fuel Cells (MFCs) with Manganese Dioxide (MnO<sub>2</sub>) Cathodes," *Biotechnological Engineering Journal*, Vol. 54, No. 1, 2011, pp. 10-15. <http://dx.doi.org/10.1016/j.bej.2011.01.001>
- [7] S. L. Suib, "Porous Manganese Oxide Octahedral Molecular Sieves and Octahedral Layered Materials," *Accounts of Chemical Research*, Vol. 41, No. 4, 2008, pp. 479-487. <http://dx.doi.org/10.1021/ar7001667>
- [8] J. Yuan, K. Laubernds, J. Villegas, S. Gomez and S. L. Suib, "Spontaneous Formation of Inorganic Paper-Like Materials," *Advanced Materials*, Vol. 16, No. 19, 2004, pp. 1729-1732. <http://dx.doi.org/10.1002/adma.200400659>
- [9] J. A. Rogers, M. G. Lagally and R. G. Nuzzo, "Synthesis, Assembly and Applications of Semiconductor Nanomembranes," *Nature*, Vol. 477, No. 7362, 2011, pp. 45-53. <http://dx.doi.org/10.1038/nature10381>
- [10] S. I. A. Razak, S. H. S. Zein and A. L. Ahmad, "MnO<sub>2</sub>-Filled Multiwalled Carbon Nanotube/Polyaniline Nanocomposites: Properties and Its Percolation Threshold," *Nano: Brief Reports and Reviews*, Vol. 6, No. 1, 2011, pp. 81-91. <http://dx.doi.org/10.1142/S1793292011002378>
- [11] J. Roller, R. Neagu, F. Orfino and R. Maric, "Supported and Unsupported Platinum Catalysis Prepared by a One-Step Dry Deposition Method and Their Oxygen Reduction Reactivity in Acidic Media," *Journal of Materials Science*, Vol. 47, No. 11, 2012, pp. 4604-4611. <http://dx.doi.org/10.1007/s10853-012-6324-3>
- [12] R. Maric, J. Roller and R. Neagu, "Flame-Based Technologies and Reactive Spray Deposition Technology for Low-Temperature Solid Oxide Fuel Cells: Technical and Economic Aspects," *Journal of Thermal Spray Technology*, Vol. 20, No. 4, 2011, pp. 696-718. <http://dx.doi.org/10.1007/s11666-011-9645-x>
- [13] R. Maric, K. Furusaki, D. Nishijima and R. Neagu, "Thin Film Low Temperature Solid Oxide Fuel Cell (LT-SOFC) by Reactive Spray Deposition Technology (RSDT)," *ECS Transactions*, Vol. 35, No. 1, 2011, pp. 473-481.
- [14] R. Maric, R. Neagu, Y. Zhang-Steenwinkel, F. Van Berkel and B. Rietveld, "Reactive Spray Deposition Technology—An One-Step Deposition Technique for Solid Oxide Fuel Cell Barrier Layers," *Journal of Power Sources*,

- Vol. 195, No. 24, 2010, pp. 8198-8201.  
<http://dx.doi.org/10.1016/j.jpowsour.2010.06.053>
- [15] R. Nédélec, R. Neagu, S. Uhlenbruck, R. Maric, D. Sebold, H. Buchkremer and D. Stöver, "Gas Phase Deposition of Diffusion Barriers for Metal Substrates in Solid Oxide Fuel Cells," *Surface & Coatings Technology*, Vol. 205, No. 16, 2011, pp. 3999-4004.  
<http://dx.doi.org/10.1016/j.surfcoat.2011.02.021>
- [16] J. Roller, "Low Platinum Electrodes for Proton Exchange Fuels Cells Manufactured by Reactive Spray Deposition Technology," MSc Thesis, University of British Columbia, Vancouver, 2009.
- [17] A. Camenzind, W. R. Caseri and S. E. Pratsinis, "Flame-Made Nanoparticles for Nanocomposites," *Nano Today*, Vol. 5, No. 1, 2010, pp. 48-65.  
<http://dx.doi.org/10.1016/j.nantod.2009.12.007>
- [18] T. T. Kodas and M. J. Hampden-Smith, "Aerosol Processing of Materials," Wiley-VCH, New York, 1999.
- [19] P. Roth, "Particle Synthesis in Flames," *Proceedings of the Combustion Institute*, Vol. 31, No. 2, 2007, pp. 1773-1788. <http://dx.doi.org/10.1016/j.proci.2006.08.118>
- [20] R. Strobel and S. E. Pratsinis, "Flame Aerosol Synthesis of Smart Nanostructured Materials," *Journal of Materials Chemistry*, Vol. 17, No. 45, 2007, pp. 4743-4756.  
<http://dx.doi.org/10.1039/b711652g>
- [21] M. S. Wooldridge, "Gas-Phase Combustion Synthesis of Particles," *Progress in Energy and Combustion Science*, Vol. 24, No. 1, 1998, pp. 63-87.  
[http://dx.doi.org/10.1016/S0360-1285\(97\)00024-5](http://dx.doi.org/10.1016/S0360-1285(97)00024-5)
- [22] K. Wegner and S. E. Pratsinis, "Nozzle-Quenching Process for Controlled Flame Synthesis of Titania Nanoparticles," *AIChE Journal*, Vol. 49, No. 7, 2003, pp. 1667-1675.  
<http://dx.doi.org/10.1002/aic.690490707>
- [23] L. Stobinski, B. Lesiak, L. Kover, J. Toth, S. Biniak, G. Trykowski and J. Judek, "Multiwall Carbon Nanotubes Purification and Oxidation by Nitric Acid Studied by the FTIR and Electron Spectroscopy Methods," *Journal of Alloys and Compounds*, Vol. 501, No. 1, 2010, pp. 77-84.  
<http://dx.doi.org/10.1016/j.jallcom.2010.04.032>
- [24] CrystalMaker Software Ltd., "CrystalMaker: A Crystal and Molecular Structure Program for Mac and Windows," Oxford, Version 2.1.5, 1994-2009.  
<http://www.crystalmaker.com/>
- [25] R. N. DeGuzman, Y. Shen, E. J. Neth, S. L. Suib, C. O'Young, S. Levine and J. M. Newsam, "Synthesis and Characterization of Octahedral Molecular Sieves (OMS-2) Having the Hollandite Structure," *Chemistry of Materials*, Vol. 6, No. 6, 1994, pp. 815-821.  
<http://dx.doi.org/10.1021/cm00042a019>
- [26] E. Maire, N. Gimenez, V. Sauvart-Maynot and H. Sauterean, "X-Ray Tomography and Three-Dimensional Image Analysis of Epoxy-Glass Syntactic Foams," *Philosophical Transactions of the Royal Society A*, Vol. 364, No. 1838, 2006, pp. 69-88.
- [27] Q. Zhang, P. D. Lee, R. Singh, G. Wu and T. C. Lindley, "Micro-CT Characterization of Structural Features and Deformation Behavior of Fly Ash/Aluminum Syntactic Foam," *Acta Materialia*, Vol. 57, No. 10, 2009, pp. 3003-3011. <http://dx.doi.org/10.1016/j.actamat.2009.02.048>
- [28] J. Kastner, B. Harrer, G. Requena and O. Brunke, "A Comparative Study of High Resolution Cone Beam X-Ray Tomography and Synchrotron Tomography Applied to Fe- and Al-Alloys," *NDT&E International*, Vol. 43, No. 7, 2010, pp. 599-605.  
<http://dx.doi.org/10.1016/j.ndteint.2010.06.004>
- [29] L. Salvo, M. Suery, A. Marmottant, N. Limodin and D. Bernard, "3D Imaging in Material Science: Application of X-Ray Tomography," *Comptes Rendus Physique*, Vol. 11, No. 9, 2010, pp. 641-649.  
<http://dx.doi.org/10.1016/j.crhy.2010.12.003>
- [30] R. Moreno-Atanasio, R. A. Williams and X. Jia, "Combining X-Ray Microtomography with Computer Simulation for Analysis of Granular and Porous Materials," *Particuology*, Vol. 8, No. 6, 2010, pp. 81-99.  
<http://dx.doi.org/10.1016/j.partic.2010.01.001>
- [31] J. Kastner, B. Harrer and H. P. Degischer, "High Resolution Cone Beam X-Ray Computed Tomography of 3D-Microstructures of Cast Al-Alloys," *Materials Characterization*, Vol. 62, No. 1, 2011, pp. 99-107.  
<http://dx.doi.org/10.1016/j.matchar.2010.11.004>
- [32] C. Kwak, T. Park and D. J. Suh, "Preferential Oxidation of Carbon Monoxide in Hydrogen-Rich Gas over Platinum-Cobalt-Alumina Aerogel Catalysts," *Chemical Engineering Science*, Vol. 60, No. 5, 2005, pp. 1211-1217.  
<http://dx.doi.org/10.1016/j.ces.2004.07.126>
- [33] D. J. Suh, C. Kwak, J. Kim, S. M. Kwon and T. Park, "Removal of Carbon Monoxide from Hydrogen Rich Fuels by Selective Low-Temperature Oxidation over Base Metal Added Platinum Catalysts," *Journal of Power Sources*, Vol. 142, No. 1, 2005, pp. 70-74.  
<http://dx.doi.org/10.1016/j.jpowsour.2004.09.012>
- [34] H. Igarashi, H. Uchida, M. Suzuki, Y. Sasaki and M. Watanabe, "Removal of Carbon Monoxide from Hydrogen-Rich Fuels by Selective Oxidation over Platinum Catalysts Supported on Zeolite," *Applied Catalysis A: General*, Vol. 159, 1997, pp. 159-169.  
[http://dx.doi.org/10.1016/S0926-860X\(97\)00075-6](http://dx.doi.org/10.1016/S0926-860X(97)00075-6)
- [35] K. Teruuchi, H. Habazaki, A. Kawashima, K. Asami and K. Hashimoto, "Amorphous Nickel-Base Alloy Catalysts for Oxidation of Carbon Monoxide by Oxygen and Nitrogen Monoxide," *Applied Catalysis*, Vol. 76, No. 1, 1991, pp. 79-93.  
[http://dx.doi.org/10.1016/0166-9834\(91\)80006-I](http://dx.doi.org/10.1016/0166-9834(91)80006-I)
- [36] E. M. C. Alayon, J. Singh, M. Nachtgeal, M. Harfouche and J. A. Van Bokhoven, "On Highly Active Partially Oxidized Platinum in Carbon Monoxide Oxidation over Supported Platinum Catalysts," *Journal of Catalysis*, Vol. 263, No. 2, 2009, pp. 228-238.  
<http://dx.doi.org/10.1016/j.jcat.2009.02.010>
- [37] G. Gurdag and T. Hahn, "The Oxidation of Carbon Monoxide on Platinum-Supported Binary Oxide Catalysts," *Applied Catalysis A*, Vol. 192, No. 1, 2000, pp. 51-55.  
[http://dx.doi.org/10.1016/S0926-860X\(99\)00332-4](http://dx.doi.org/10.1016/S0926-860X(99)00332-4)
- [38] D. Gavril, N. A. Katsanos and G. Karaiskakis, "Gas Chromatographic Kinetic Study of Carbon Monoxide Oxidation over Platinum-Rhodium Alloy Catalysts," *Journal of Chromatography A*, Vol. 852, No. 2, 1999, pp. 507-523.  
[http://dx.doi.org/10.1016/S0021-9673\(99\)00642-1](http://dx.doi.org/10.1016/S0021-9673(99)00642-1)

- [39] M. Stancheva, S. Manev, D. Lazarov and M. Mitov, "Catalytic Activity of Nickel Based Amorphous Alloys for Oxidation of Hydrogen and Carbon Monoxide," *Applied Catalysis A: General*, Vol. 135, No. 1, 1996, pp. L19-L24. [http://dx.doi.org/10.1016/0926-860X\(95\)00275-8](http://dx.doi.org/10.1016/0926-860X(95)00275-8)
- [40] K. Wu, Y. Tung, Y. Chen and Y. Chen, "Catalytic Oxidation of Carbon Monoxide over Gold/Iron Hydroxide Catalysts at Ambient Conditions," *Applied Catalysis B: Environmental*, Vol. 53, No. 2, 2004, pp. 111-116. <http://dx.doi.org/10.1016/j.apcatb.2004.05.008>
- [41] P. V. Gosavi and R. B. Biniwale, "Catalytic Preferential Oxidation of Carbon Monoxide over Platinum Supported on Lanthanum Ferrite-Ceria Catalysts for Cleaning Hydrogen," *Journal of Power Sources*, Vol. 222, 2013, pp. 1-9. <http://dx.doi.org/10.1016/j.jpowsour.2012.07.095>

## Appendix

### Supporting Information

Formation of Platinum (Pt) Nanocluster Coatings on K-OMS-2 Manganese Oxide Membranes by Reactive Spray Deposition Technique (RSDT) for Extended Stability during CO Oxidation.

Hector F. Garces, Justin Roller, Cecil K. King'ondu, Saminda Dharmarathna, Roger A. Ristau, Rishabh Jain, Radenka Maric, Steven L. Suib\*

1) X-ray diffraction pattern of Pt nanoparticles deposited on Aluminum Stub.

The XRD pattern of the deposited Pt nanoparticles as a

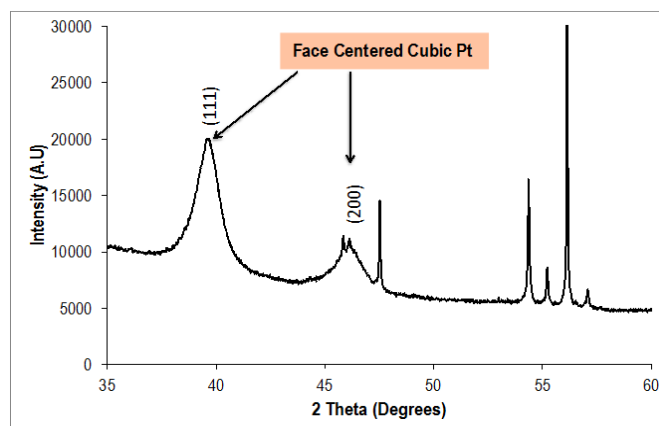


**Figure S1.** XRD patterns of face centered cubic Pt deposited on an aluminum stub during RSDT.

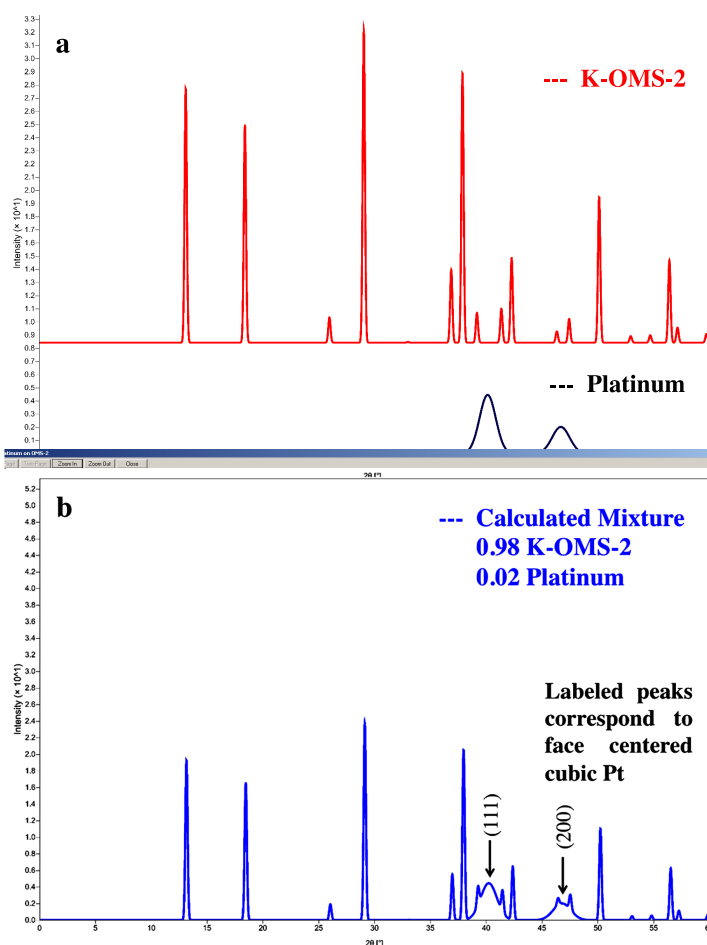


**Figure S2.** Simulated X-ray diffraction patterns of (a) K-OMS-2, and face centered cubic Pt, and (b) mixture of 0.98 K-OMS-2 plus 0.02 face centered cubic Pt.

control is presented in **Figure S1** below. The pattern is obtained for the material deposited on aluminum stub during the deposition over K-OMS-2/MWCNTs by RSDT.

2) X-ray diffraction patterns of K-OMS-2, metallic Pt,

and a mixture of K-OMS-2 and 2% face centered cubic Pt simulated by crystal maker.

3) Adsorption isotherms and pore size distribution for K-OMS-2/MWCNTs membrane and Pt deposited on K-OMS-2/MWCNTs.

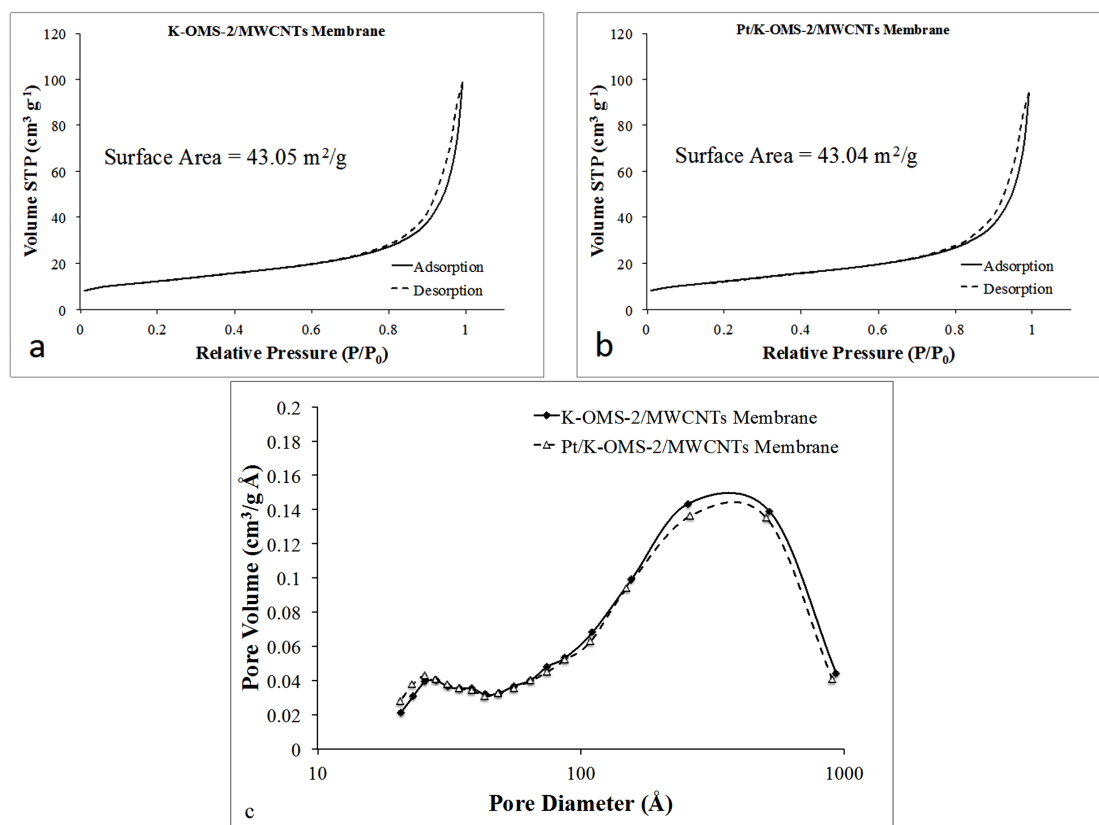


**Figure S3.** Adsorption Isotherms for (a) K-OMS-2/MWCNTs membrane, (b) Pt/K-OMS-2/MWCNTs, and (c) pore size distribution of K-OMS-2/MWCNTs Membrane and Pt/K-OMS-2/MWCNTs.

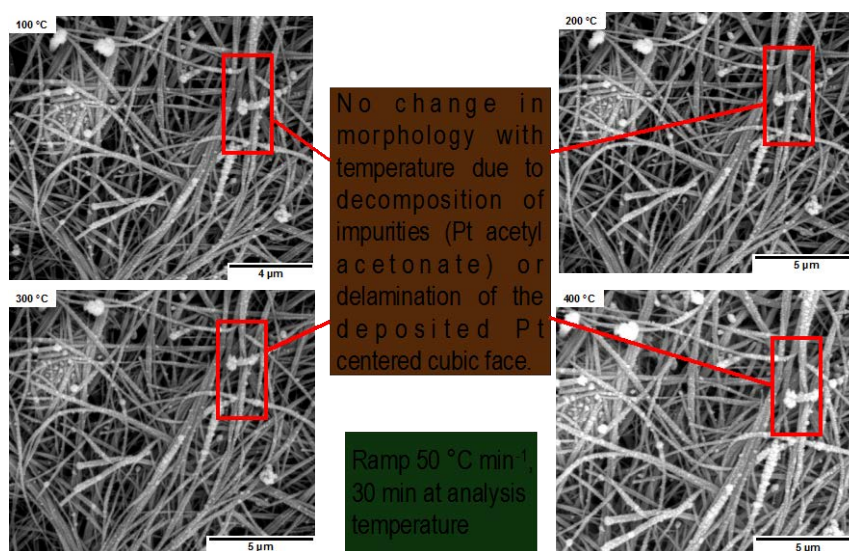


**Figure S4.** HTSEM images of coated Pt/K-OMS-2/MWCNTs at 100 °C to 400 °C ramped at 50 °C·min<sup>-1</sup> to the analysis temperature and stabilized for 30 min before obtaining the image.

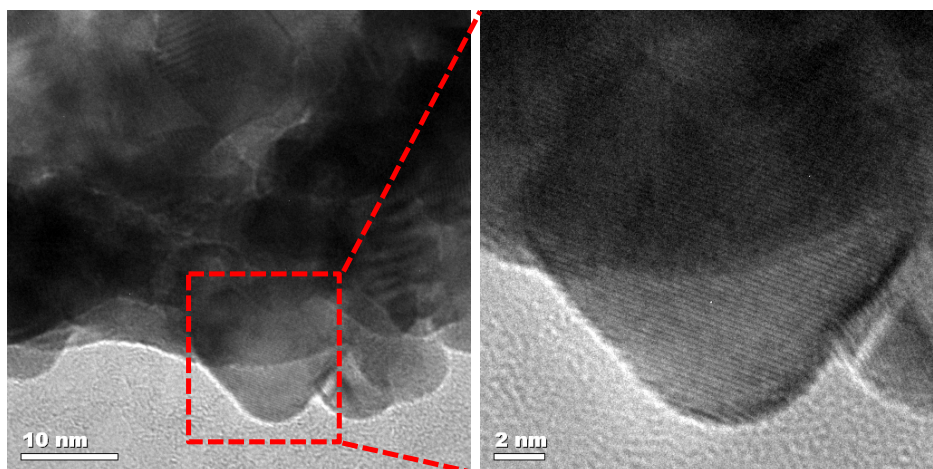


**Figure S5.** HRTEM images of coated Pt particles.

4) High Temperature Scanning Electron Microscopy (HTSEM).

*In-situ* HTSEM of coated Pt/K-OMS-2/MWCNTs sample from 100°C to 400°C showing that the film does not suffer sintering, agglomeration, delamination or there

is apparent decomposition of byproducts left after the deposition by RSDT. No depletion of the Pt particles deposited is seen.

5) HRTEM particle size Pt deposited on K-OMS-2/MWCNTs.